

Latent and Manifested flatness predictions in thin strip cold rolling using a general rolling FEM model

Sami Abdelkhalek, Hamid Zahrouni, Pierre Montmitonnet, Nicolas Legrand, Michel Potier-Ferry

▶ **To cite this version:**

Sami Abdelkhalek, Hamid Zahrouni, Pierre Montmitonnet, Nicolas Legrand, Michel Potier-Ferry. Latent and Manifested flatness predictions in thin strip cold rolling using a general rolling FEM model. 10th International Conference on Technology of Plasticity, ICTP 2011, Sep 2011, Aachen, Germany. p. 111-116. hal-00674953

HAL Id: hal-00674953

https://minesparis-psl.hal.science/hal-00674953

Submitted on 23 Aug 2012

HAL is a multi-disciplinary open access archive for the deposit and dissemination of scientific research documents, whether they are published or not. The documents may come from teaching and research institutions in France or abroad, or from public or private research centers.

L'archive ouverte pluridisciplinaire **HAL**, est destinée au dépôt et à la diffusion de documents scientifiques de niveau recherche, publiés ou non, émanant des établissements d'enseignement et de recherche français ou étrangers, des laboratoires publics ou privés.

Latent and Manifested Flatness Predictions in Thin Strip Cold Rolling: Comparison of Coupled and non-Coupled FEM Approaches

S. Abdelkhalek[1,2,3)], H. Zahrouni[1)], P. Montmitonnet[2)*], N. Legrand[3)], M. Potier-Ferry[1)]

[1)] Laboratoire d'Etude des Microstructures et de Mécanique des Matériaux (LEM3, UMR CNRS 7239), Université Paul Verlaine, Metz / France; [2)] Centre for Materials Forming (CEMEF, UMR CNRS 7635), MINES-ParisTech, Sophia-Antipolis / France; [3)] ArcelorMittal Research Maizières, R&D Industrial Operations, Maizières-les-Metz / France

* Corresponding author: E-mail address: Pierre.montmitonnet@mines-paristech.fr ; Tel.: +33 4 93 95 74 14

Abstract

Flatness defects in thin strip cold rolling are a consequence of roll thermo-elastic deformation and the resulting heterogeneous strip plastic deformation. But in the case of on-line, manifested flatness defects, buckling reorganizes the stress field in the pre- and post-bite areas, which might impact strain and stress fields *in* the bite or at its ends. Such effects have always been neglected in the past. The purpose of the present paper is to present two *coupled* approaches to examine to what extent such potential in-bite / out-of-bite feedback determines the in-bite fields and the flatness of the strip. Using both methods and comparing with the standard case where buckling is not accounted for, it has been shown that (i) taking buckling into account results in completely different stress fields and fits correctly the measured on-line residual stresses under tension ("stress-meter rolls"); (ii) coupling buckling in the post-bite area and the rolling model, whatever the technique, changes little the in-bite fields; differences, if any, concentrate in the immediate vicinity of the bite exit; (iii) but in the case where manifested flatness defects occur, these tiny interactions (namely, through the exit velocity transverse profile) are essential for the precise description of the residual stresses and for accurate flatness prediction.

Keywords: Cold strip rolling, Buckling, Flatness defects, 3D FEM, Shell FEM, Asymptotic Numerical Method

Introduction

Due to rolls deforming elastically, the roll gap is not uniform in the width direction. As a result, strip reduction slightly depends on the width coordinate y. This induces residual stresses which, for thin strips, may be compressive locally in spite of the strip tension applied. In such cases, on-line manifested flatness defects may occur (**Fig. 1**). These are non developable, out-of-plane displacements due to elastic or plastic buckling, mostly in the form of periodic waves (centre waves, edge waves…).

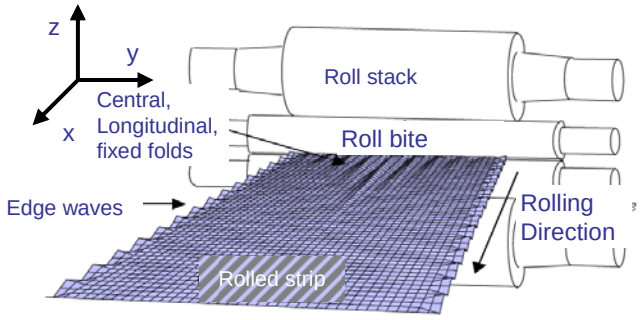


Figure 1. Flatness defects.

Even in the case where the strip tension is high enough to maintain the strip flat (i.e. avoid buckling), residual stresses are present. The profile $\sigma_{xx}(y)$ can be measured using stress-meter rolls located beyond the stand. When the strip tension is relaxed, they may induce buckling and flatness defects. This is the reason why such stress profiles are called "latent flatness defects".

Flatness defects are a major problem encountered on hot strip mills, and still worse on cold mills – the thinner the strip, the easier buckling is. It is essential to model their occurrence and severity, and investigate their correction using flatness actuators such as roll bending.

If defects are only latent, the stress field computed beyond the bite by e.g. a 3D FEM model should be correct. In such a case, buckling upon unloading the strip tension is generally dealt with using uncoupled approaches: the stress pattern computed by the strip rolling model are transferred into a buckling (shell) model, which tells if the critical conditions for buckling are met, and computes post-buckling data (wavelength, amplitude of defects).

However, if defects are manifested on-line, the stress field is completely transformed; as will be shown, the solution coming out of the 3D FEM is completely irrelevant beyond the bite – i.e. where buckling occurs. Furthermore, the question arises of the impact of this stress reorganization on the strains and stresses *within* the bite. The purpose of the present paper is therefore to describe and apply two *coupled* rolling / buckling models, to address the abovementioned issue.

Literature survey

A number of uncoupled techniques have been presented in the literature. The standard solution of Timoshenko and Woinovsky-Krieger (1940) solves the von Karman equation for a rectangular plate, assuming sinusoidal waves in both x and y directions, and clamping boundary conditions. The critical load depends on the width-to-length ratio, the wavelength is of the order of the width.

This model is built for plate buckling under homogeneous stress boundary conditions, and is not adapted to the complex fields of strip rolling. Several authors have extended it to loadings consisting in a stress *profile* along the width. Bush et al. (2001) assume sinusoidal waves in the length (rolling) direction, and a stripwise-defined bound-

ary stress profile across the width. The assumed out-of-plane displacement field is introduced into von Karman's equation; the critical load parameter and the transverse shape are computed by solving a boundary value problem, and the wavelength is the one giving the lowest critical load.

Only right/left symmetric waves are addressed, whereas real waves are often anti-symmetric. This has been recognized by Fischer et al. (2003), who allowed the transverse shape to be either an odd or an even polynomial in y, while remaining sinusoidal in the rolling direction. They determined the strip shape by minimizing the elastic energy of the deformation path from flat to wavy shape.

The latter two are useful, semi-analytical models for edge waves or centre waves only, since only the longitudinal stress component is used. Moreover, the type of defect (centre or edge wave) is determined *a priori* from the shape of the stress profile, and *ad hoc* boundary conditions are applied to get it in the end.

Yukawa et al. (1986) were among the first to address more complete configurations using numerical (shell FEM) modelling. This was also a non-coupled approach, involving a buckling and a post-buckling analysis. Importing the stress field from rolling, the bifurcation point is detected as the load parameter which leads to a non-definite positive second variation of the total elastic strain energy (or stiffness matrix), the strip being assumed flat (out-of-plane displacement w = 0). This is an eigenvalue problem, the principal vector of which gives the buckling mode. Then a small defect corresponding to this mode is added to the strip geometry; the calculation is restarted with free w(x,y) to give the post-buckled shape and stress, the load step being controlled by a modified Riks method.

Abdelkhalek et al. (2009) have described a similar non coupled approach using shell FEM, but where the loading steps are managed by the Asymptotic Numerical Method (Zahrouni et al., 1999, Boutyour et al., 2004). The latter consists in developing the solution (displacement and load parameter) in a power series with respect to a step length parameter, up to a truncation order *p*. Inserting this series in the non linear equations of the problem and identifying the different orders, results in a succession of *p* linear systems with the same tangent stiffness matrix, and right-hand side vectors computed from the solutions at lower orders. This allows maximizing the load step and decreasing the computational burden. They modelled both the on-line shape (under strip tension) and the relaxed shape, once strip tensions are relieved, whereas the previous papers dealt only with the latter.

Counhaye (2000) was the first to question the decoupling of the rolling and the buckling model. Using an approach similar to Roddeman et al. (1987a, 1987b), he considered buckling as one more component, present only in the out-of-bite areas, to be added to the elastic and the plastic strain rate decomposition. An equivalent strain rate was therefore added, which represents the local shortening of a segment due to buckling. Namely, the waviness reduces the distance $\widetilde{L}$ between the ends of the segment, whereas the material, non-straight length remains L (to a small elastic strain). This can be seen as a decrease of the elastic stiffness, applied wherever the stress is more negative than a critical bucking stress, moreover taken very small (the approach is therefore valid for thin strips).

This approach is quite simple to implement, being a modification of the constitutive models, where negative stresses are eliminated by computing the $\lambda = \mathrm{Ln}(\widetilde{L}/\mathrm{L})$ strain which cancels them. On the other hand, this way of doing deals with buckling on a material point basis, whereas it is in fact possible only on a certain area, of the order of the wavelength of the eigen-displacement.

Two coupled rolling / buckling models

Based on ideas presented above, the present paper introduces two algorithms coupling buckling and rolling models, which will be compared in the next sections. The rolling model is Lam3/Tec3, a strip / roll stack deformation model described in Hacquin et al. (1995, 1998); its general flow chart is given in **Fig. 2**. This implicit software uses a *steady state* formulation based on streamline integration. The roll stack deformation model is based on advanced beam theory, Boussinesq solution of a half-space under general loading, and Hertz contact mechanics.

The first buckling model is inspired from Counhaye (2000), and has been implemented in Lam3/Tec3, forming a strongly coupled model of rolling with buckling, called later L3T3-C.

The second one is the Asymptotic Numerical Method (ANM) described above in the non-coupled context; here, it is coupled in a staggered scheme with Lam3/Tec3, giving L3T3-ANM.

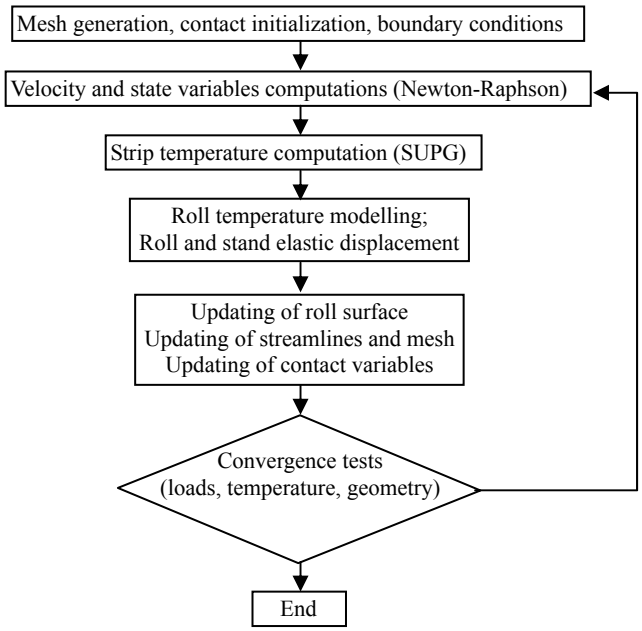


Figure 2. General algorithm of Lam3/Tec3 FEM strip rolling model.

Integrating buckling at the material behaviour level. This coupling has been detailed in Abdelkhalek et al. (2010a). Here, only the flowchart is recalled, **Fig. 3**. Stresses are tested everywhere outside the bite. If a compressive in-plane stress is found on an element (averaged over the thickness), the eigen-directions of stress are de-

termined, the computation of the λ's is activated, the (elastic) strain increment is corrected from the "buckling shortening", and sent back to the next Newton-Raphson iteration for the stress increment determination. This analysis gives both the local shortening due to buckling, indicating wave formation, and the eigen-directions, giving the orientation of the waves (centre or edge waves, longitudinal waves or "towel effect", see **Fig. 1**, or even transverse waves (herringbone, quarterbuckles…). Nothing is found on wavelength or amplitude; simply, the amount of shortening tells about the severity of the defect, qualitatively.

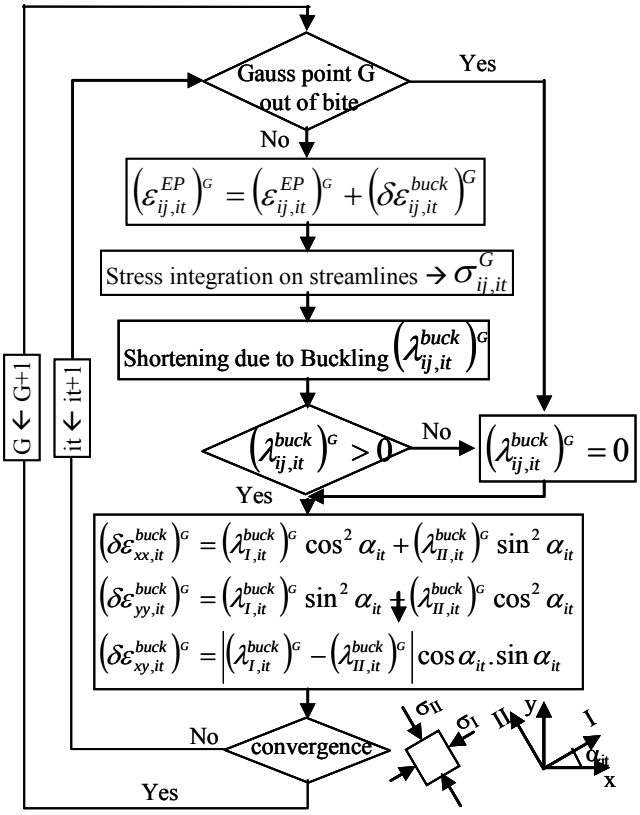


Figure 3. Flow-chart of the constitutive model solution in the coupled rolling / buckling model Lam3/Tec3-Counhaye or L3T3-C.

Coupling 3D FEM and Asymptotic Numerical Method shell FEM. Here, the principle is very different. A full Lam3/Tec3 simulation is run, until all iteration loops come to a converged solution. Then, the post-bite stress field is interpolated on the shell element mesh of the ANM buckling model. Note that:

– The whole stress field (σ_{xx}, σ_{yy}, σ_{xy}) may be transferred; furthermore, it may be transferred starting at the very edge of the bite, whereas all previous models used only the stabilized stress field, hundreds of mm after bite exit. It is quite important to involve this very complex bite vicinity area, where very strong stress gradients exist, the impact of which has to be tested.

– As very large gradients are present on the edge of the strip, a very precise interpolation scheme has to be used. Here, a Moving Least Squares method has been developed, with optimization of the shell mesh density and of the extension of the weight functions associated with shell Gauss points (Abdelkhalek, 2010b).

After this transfer step, a buckling and post-buckling analysis is performed by the ANM; this in particular changes the stress state in the post-bite part of the system, including the exit line of the bite (which is the upstream edge of the shell mesh). This is considered as a novel boundary condition on the 3D FEM computation of strip and roll deformation. Its mesh is truncated at bite exit, and the abovementioned modified stresses are applied. Lam3/Tec3 is run again in this new configuration, giving a slightly modified strip and roll deformation and stress pattern. Before going back to shell buckling, a new stress field must be computed for the post-bite area: this is done using another Lam3/Tec3 simulation, on a complete mesh this time, but using only the last deformed roll stack. This puts an end to the corresponding iteration of the staggered scheme, and the whole procedure is repeated until convergence. In fact, coupling happens to be weak, convergence is always reached at the third global iteration at most.

This is a somewhat complex scheme, introducing possible information loss during transfers. The advantage is that the buckling model is highly powerful and reliable.

Results

The two schemes will now be compared on a typical rolling pass on thin steel strip, described in **Table 1**, a case with large roll deformation (especially roll flattening). A 6200-node hexahedral mesh has been used after optimization; it is strongly refined at bite inlet and exit, and also near the edge where the element width is 1 mm.

Table 1. Characteristics of strip rolling pass investigated.

Strip width	855 mm
Entry strip thickness (strip crown)	0,355 mm (4.81 %)
Exit thickness	0,252 mm
Rolling speed	22 m/s
Front / back tension	100 MPa / 170 MPa
Type of mill diameters WR / BUR Length WR/BUR	4-high 555mm / 1300mm 1400mm / 1295mm
Work Roll / Back-Up Roll crown	0.0322 % / No crown
Counterbending force / position	4.8 MN / y = 1010 mm
Screwdown force application	y = 1075 mm
Friction law : Coulomb	$\tau = 0,03 \times \sigma_n$
Strip material behaviour: Young's modulus, Poisson's cœfficient, Strain hardening (MPa)	E = 210 GPa,: ν = 0,3 $\sigma_0 = (470.5 + 175.4.\bar{\varepsilon}) \times$ $(1 - 0.45.\exp(-8.9\bar{\varepsilon}))$ -175

First, a short analysis is given of the results of the computation without buckling. **Fig. 4** shows the longitudinal stress field $\sigma_{xx}(x,y)$ up to ≈50 mm from the edge; in the rolling direction, the displayed area extends ~40 mm before and after the bite. The latter is marked by a very compressive stress; the minimum – 1300 MPa is found 5 mm from the edge. This profile is characteristic of the edge-drop defect, i.e. the transition between the deformed and non-deformed zones of the roll.

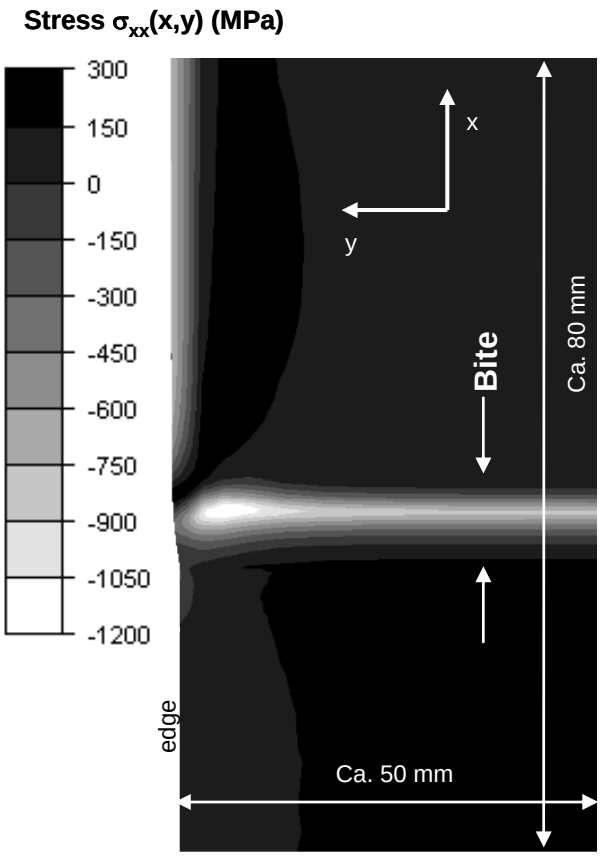


Figure 4. $\sigma_{xx}(x,y)$ stress field resulting from Lam3/Tec3-standard (without buckling model).

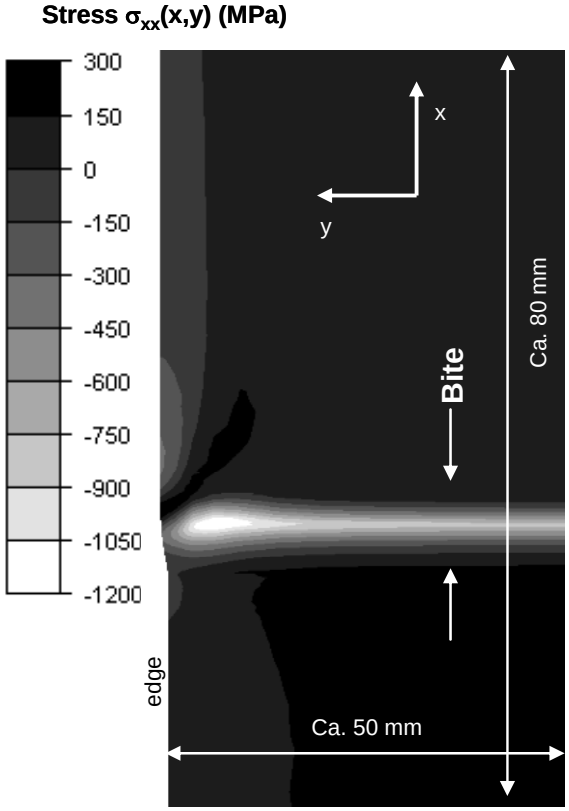


Figure 5. Stress map with buckling modelled by L3/T3-C.

The local reduction results from the incoming strip crown and the deformed roll profile. It is maximal on the edge, which is therefore the most elongated area in the bite. The stress near the edge (4-5 mm in the y-direction) is mostly compressive in the bite; it briefly turns tensile by the end of the contact, then becomes strongly compressive and falls down to -770 MPa, maintained all down the line after the bite, as shown by **Fig. 6** below, case "Lam3/Tec3 standard". **Fig. 6** pictures stress profiles $\sigma_{xx}(y)$ nearly 1m after the bite, where a stress-meter roll is located. The average of this stress distribution is 100 MPa, the strip tension stress. The distribution is obviously in complete disagreement with the experimental profile.

Impact of buckling on post-bite stress map $\sigma_{xx}(x,y)$. Now, the buckling models are introduced for comparison. **Fig. 5** shows a stress map equivalent to **Fig. 4**, but with L3T3-C; the areas displayed and the colour scale are almost the same. The stress σ_{xx} shows a large difference only in the out-of-bite areas. Except in a 20 mm long x 5 mm wide zone just after bite exit, the compressive stress on the edge has disappeared. It has been relaxed by local buckling, to be displayed in a later section.

Impact of buckling on remote stress profile $\sigma_{xx}(y)$. The remote σ_{xx} profiles are completely transformed (**Fig. 6**), homogenized in a rather similar way by both coupled models. Small differences appear however:

- Near the edge, L3T3-ANM gives a slightly tensile stress, where L3T3-C gives -50 MPa on a very narrow, 3 mm width. As the measurement does not extend to this area, there is no definitive argument in favour of one model or the other.
- In the centre, L3T3-C gives a slightly better agreement with experiments. This may look anecdotic, but the buckling mode of such thin strips proves to be very sensitive to this ≈10 MPa difference. Here, the strong coupling of L3T3-C may be the reason for its better agreement.

It is interesting to compare these profiles with a non-coupled chaining of Lam3/Tec3 with the ANM method (transfer of Lam3/Tec3 stress map to the ANM shell model and buckling + post-buckling computation, without feedback to the rolling model). The relaxed profile is quite different, and farther from the experiment. Therefore, even if the buckling-induced relaxation does not change the in-bite fields, the absence of coupling results in inexact stress profiles – and potentially wrong buckling mode.

Impact of buckling on velocity field. Fig. 7 plots the $v_x(y)$ velocity profile on the exit line (which is in fact curved due to roll deformation). It shows that due to the larger reduction near the edge, the exit material velocity is slightly larger (1%) near the edge. Farther away from the bite, a rigid-body movement has to be retrieved. This velocity profile evolution, with the edge being slowed down while the centre is accelerated, is another visualization of the compression of the edges which leads to buckling.

The application of the buckling algorithms, strongly coupled or staggered, tends to flatten this profile except in the extreme vicinity (1 mm) of the edge. This is what

makes the simple chaining of rolling and buckling models different from coupled approaches.

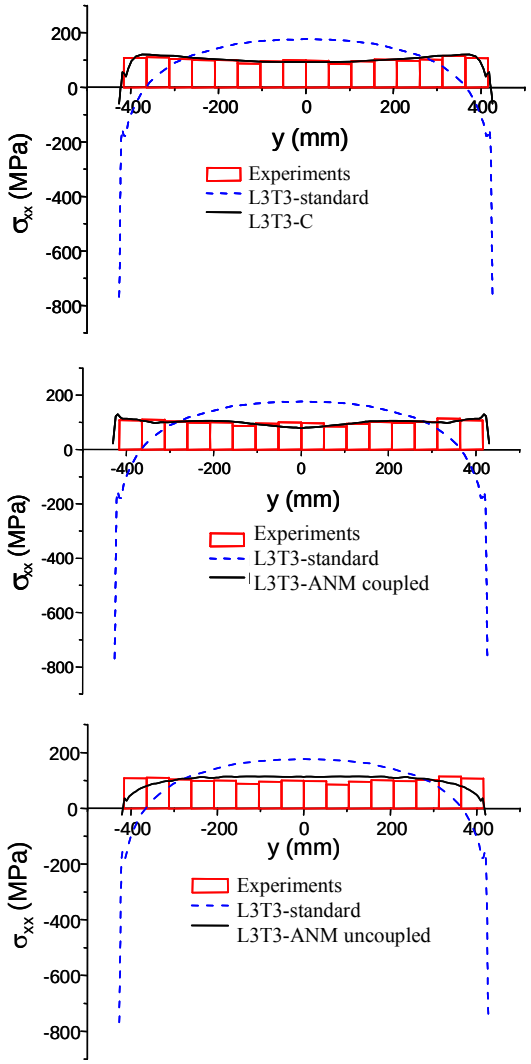


Figure 6. Remote stress profiles at the position of the stress-meter roll, comparing experiments with Lam3/Tec3 standard (without buckling model), L3T3-C and L3/T3-ANM, and the non coupled Lam3/Tec3 + ANM chaining.

An important result is that these changes in both the stress pattern after the bite and the velocity profile on the exit line have no significant influence on the strain and stress pattern *inside* the bite, and as a consequence, on the roll deformation. This conclusion is not absolutely general: for a small deformation pass, some impact on in-bite stress and velocity has been detected, after the neutral point; however, until now, the impact on roll deformation has been found insignificant in all cases (Abdelkhalek, 2010b).

On-line and tension-relaxed shape defects. There remains to examine the flatness defects predictions. **Fig. 8** gives the predictions of L3T3-ANM. Under tension, only longitudinal (steady state) waves are present near the centreline. They are not flatness defects, but a "towel effect", not entrained with the strip. The edges are "clean".

On the contrary, defects appear when strip tension is cancelled, both a centre wave (wavelength 500 mm, amplitude 4 mm) and a wavy edge (wavelength 150 mm, amplitude 2 mm). Interestingly, the centre wave appears almost immediately after bite exit, whereas the edge wave starts only 180 mm after bite exit. This question of the onset of the defects is not essential in practice, but quite important for future validation of the models.

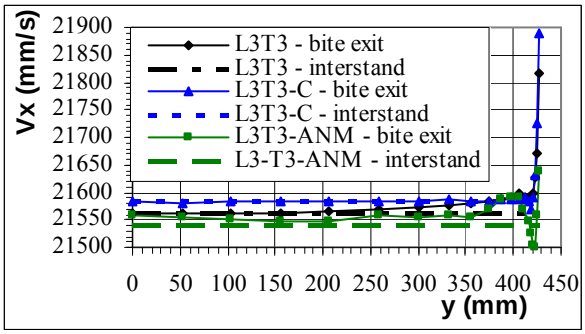


Figure 7. V_x velocity component just at the exit of the bite, and at the position of the stress-meter roll. Comparison of Lam3/Tec3 (without buckling model), L3/T3-C and L3/T3-ANM.

In **Fig. 8**c, the non-coupled, chained rolling + buckling model has been used for comparison. It shows the same edge wave; however, the centre wave does not appear.

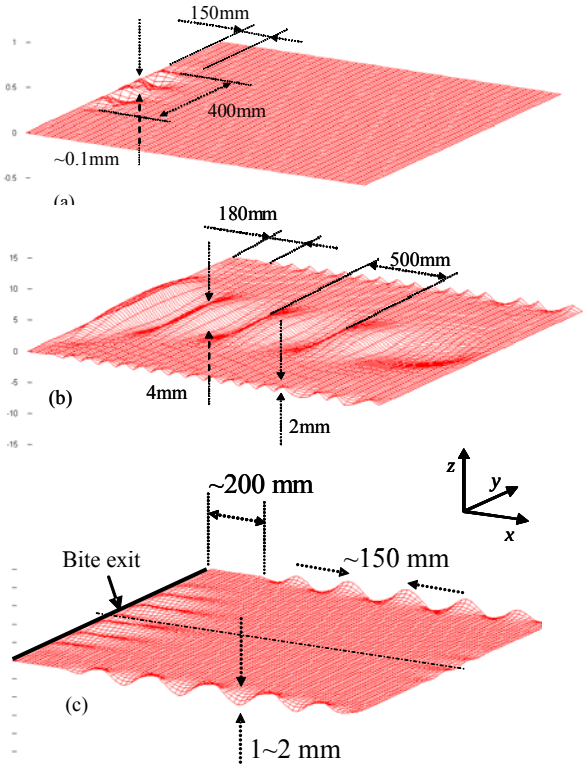


Figure 8. Strip shape computed by L3/T3-ANM. Computation has been done on half the width and symmetrized for better visualization. (a) On-line (under strip tension); (b) relaxed. (c) Non-coupled computation, tension relaxed.

L3T3-C (**Fig. 9**) can predict shape defects only under tension. Here, a wavy edge is predicted (non-zero λ_I). Some longitudinal waves at bite exit ("towel effect") are detected also by the non-zero λ_{II} (not shown here), but these are not flatness defects properly speaking.

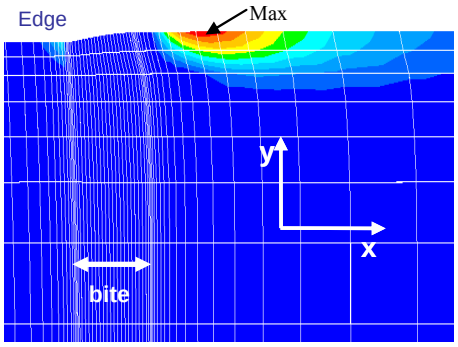


Figure 9. Strip shape computation in L3/T3-C, λ_l = shortening along x; maximum (red) is 1.5 10^{-3}, minimum (deep blue) is 0. Only the vicinity of the edge is shown. White lines are the mesh; the bite, marked by a refined meshing, is 9 mm long.

Discussion

Some differences arise between the two coupled models. Unfortunately, only a very qualitative observation on the mill is available from Counhaye (2000), from which this rolling pass has been taken. He states that short-wavelength, small-width waves were present (under tension). This tends to support the fully coupled model against the staggered one, although more powerful in terms of buckling modelling. Also, it can be seen in **Fig. 6** that subtracting the strip tension stress (100 MPa) leaves the L3T3-C profile positive in the centre, whereas the profile by L3T3-ANM goes negative. This explains the occurrence of the centre wave, not mentioned from observation on the mill. Small as this difference may seem, it is probably significant for practical results. As for the chained model, its convex stress profile in **Fig. 6** leads to a positive stress in the centre after tension cancelling, hence the absence of centre wave.

Conclusion

The comparison of the two coupled models (and a non-coupled version Lam3/Tec3 → ANM as well) shows that a strong coupling of the two models is necessary. In some cases (very low reduction), some changes in the in-bite fields has been found, without impact however on the roll deformation. But the exit velocity field is always subtly modified; this is suggested to be a major driving force for the stress changes in the immediate post-bite zone, and to influence in all cases the strip buckling mode.

Different limitations should be overcome in the future:

- Strong coupling is necessary, as well as a good buckling and post-buckling description. A better solution would be e.g. to couple Lam3/Tec3 and the ANM model by a powerful hybridization method such as Arlequin (Ben Dhia and Rateau, 2005).
- Some very short and narrow waves may be buckling in the plastic state, which suggests to use an ANM version adapted to the non-linear constitutive model.

Finally, for a complete assessment of the models presented here and the present conclusions, it would be necessary to compare not only stress profiles (far from the bite), but also wave shapes (in particular just at bite exit, where they form). The present authors and colleagues are presently doing such an experimental effort.

Acknowledgement

The authors are indebted to ArcelorMittal for financial support of this work and permission to publish it.

References

Abdelkhalek, S., Zahrouni, H., Potier-Ferry, M., Montmitonnet, P., Legrand, N., Buessler, P., 2009. Modélisation numérique du flambage des plaques minces et application au laminage. In: Proc. (CD-ROM) CFM 2009, August 24-28, Marseille, France, 6 p. (in French).

Abdelkhalek, S., Montmitonnet, P., Potier-Ferry, M., Zahrouni, H., Legrand, N., Buessler, P., 2010a. Strip flatness modelling including buckling phenomena during thin strip cold rolling. Ironm. Steelm. 37, p. 290-297.

Abdelkhalek, S., 2010b. Un exemple de flambage sous contraintes internes : étude des défauts de planéité en laminage à froid des tôles minces, Ph.D. dissertation, Ecole des Mines de Paris (in French).

Ben Dhia, H., Rateau, G., 2005. The Arlequin method as a flexible engineering design tool. Int. J. Num. Meth. Engg 62 (11), p. 1442-1462.

Boutyour, E.H., Zahrouni, H., Potier-Ferry, M., Boudi, M. 2004. Bifurcation points and bifurcated branches by an Asymptotic Numerical Method and Padé approximants. Int. J. Num. Meth. Engg, 60, p. 1987-2012.

Bush, A., Nicholls, R., Tunstall, J., 2001. Stress levels for elastic buckling of rolled strip and plate, Ironm. Steelm. 28, p. 481-484.

Counhaye, C., 2000. Modélisation et contrôle industriel de la géométrie des aciers laminés à froid, PhD Dissertation, University of Liège (in French).

Fisher, F.D., Rammerstorfer, F.G., Friedl, N., 2003. Residual stress-induced centre wave buckling of rolled strip metal. ASME J. Appl. Mech. 70, p. 84-90.

Hacquin, A., Montmitonnet, P., Guillerault, J.-P., 1995. Coupling of roll and strip deformation in 3D simulation of hot rolling. In: Proc. NUMIFORM 95, June 18-21, Ithaca, NY, USA, p. 921-927.

Hacquin, A., Montmitonnet, P., Guillerault, J.-P., 1998. A 3D semi-analytical model of rolling stand deformation with finite element validation. Eur. J. Mech. - A : Solids 17 (1), p. 79-106.

Roddeman, D.G., Drukker, J., Oomens, C.W.J., Janssen, J.D., 1987a,b. The Wrinkling of Thin Membranes, Part I- Theory. ASME J. Appl. Mech. 54, p. 884-887. Part II- Numerical Analysis. ASME J. Appl. Mech. 54, p. 888-892.

Timoshenko, S., Woinovsky-Krieger, S., 1940. Theory of plates and shells, McGraw-Hill Book Co., New York.

Yukawa, N., Ishikawa, T., Tozawa, Y., 1986. Numerical analysis of the shape of rolled strip. In: Proc. NUMIFORM Conference, August 25-29, Gothenburg, Sweden, p. 249-254.

Zahrouni, H., Cochelin, B., Potier-Ferry, M., 1999. Computing finite rotations of shells by an Asymptotic-Numerical Method, Comp. Meth. Appl. Mech. Engg 175 (1-2), p. 71-85.